3.5 Shock joining

There will be a section on numerical methodology and it is cited several times in this section. Need to fill in the correct section number when this is done.

The reader of Sections 3.3 and 3.4 has seen a variety of shock waves, or 'shocks', composed of abrupt or discontinuous changes in the depth or width of the flow within which the semigeostrophic and/or hydrostatic approximations break down. Examples include the advancing Kelvin wave bores in the Rossby adjustment problem (Figures 3.3.6 and 3.3.7), the Kelvin wave hydraulic jump and upstream bore (Figure 3.4.11) and the transverse hydraulic jumps and bores (Figure 3.4.8, 3.4.9, and 3.4.12). We now make a closer examination of these features by exploring the relationship between the flow immediately upstream and downstream. Begin by considering a hypothetical discontinuity in fluid depth occurring along a contour C (Figure 3.5.1). For the time being, it will be assumed that the fluid depth remains non-zero over C. Away from C the fluid motion is governed by the shallow water equations. If the system is one of reduced gravity, where the moving surface is an interface separating fluids of different densities, then the discontinuity may be associated with mixing of the two fluids. Investigators of non-rotating, internal shocks are still working on a satisfactory way of dealing with this *diapycnal* mixing. We will neglect any such mixing.

There are (at least) two methods for obtaining the matching conditions across a discontinuity of depth. The first and most popular approach is to write down the equations of motion in a' flux' form that insures that the discontinuity contains no sources of mass or momentum. The flux form of the y-momentum equation was discussed briefly in Section 1.6 and we generalize that result to two dimensions. To obtain matching conditions on u, v, and d, the flux equations are integrated across the shock. These equations are also commonly used as a basis for numerical integration of the shallow water equations in situations where shocks arise (see Section *on numerical methods*). A second approach is to formulate the primitive conservation statements on mass and momentum over a control volume containing the discontinuity. This method is more fundamental and direct. It yields the same results as the flux form of the shallow water equations; the latter are, after all, based on the same control volume relations. The following discussion is based on Pratt (1983b) and Schär and Smith (1993) although some of the basic ideas can be traced back to Crocco (see Batchelor, 1967 Section 3.5).

It is assumed, then, that the discontinuity (shock) contains no sources nor sinks of mass and that it occurs over a distance sufficiently short that momentum sources such as bottom drag or bottom slope are negligible. It will be helpful to use a Cartesian coordinate system (n,s), placed such that n is aligned normal to and s perpendicular to C at the point P (Figure 3.5.1). The coordinate system remains fixed but C moves at speed $c^{(n)}$ in the n-direction. Integration of the dimensionless continuity equation (2.1.7) over a small interval $[-\varepsilon \le n \le \varepsilon]$ about the shock at this point results in

$$\int_{-\varepsilon}^{\varepsilon}\frac{\partial d}{\partial t}dn+\left[u^{(n)}d\right]_{n=\varepsilon}-\left[u^{(n)}d\right]_{n=-\varepsilon}+\int_{-\varepsilon}^{\varepsilon}d\frac{\partial u^{(s)}}{\partial s}dn=0\,. \qquad (3.5.1)$$

The first integral can be written as

$$\frac{\partial}{\partial t}\int_{-\varepsilon}^{\varepsilon}(d)dy=\frac{\partial}{\partial t}\int_{-\varepsilon}^{n_c(t)}(d)dy+\frac{\partial}{\partial t}\int_{n_c(t)}^{\varepsilon}(d)dy$$

where n_c(t) is the position of the discontinuity on the n-axis. If ε is reduced to zero the right-hand side approaches $-c^{(n)}\langle d\rangle$, where $c^{(n)}=\partial n_c/\partial t$ and $\langle d\rangle$ is the change in d across the discontinuity, expressed using the shorthand $\langle(\ )\rangle=\lim_{\varepsilon\to 0}[(\ )_\varepsilon-(\ )_{-\varepsilon}]$. Since the shock is parallel to the n-axis, the s-derivative in (3.5.1) is bounded along this integration path and the final integral of can be made arbitrarily small by letting ε approach zero. The general constraint imposed by mass conservation can thus be written as

$$c^{(n)}\langle d\rangle-\langle u^{(n)}d\rangle=0 \qquad (3.5.2).$$

The same approach may be taken with regard to momentum, but care must be exercised in choosing the correct form of the momentum equations to integrate across the shock. For example, (2.1.5) and (2.1.6) express momentum conservation at particular level z with in the fluid, and integration across the shock would presume that that there are no sources of horizontal momentum at each value of z within[1]. In fact, one can only be certain that no sources of momentum can act on the depth integrated flow as a whole. We therefore consider the depth-integrated versions of (2.1.5) and (2.1.6), formed by multiplying the latter by d and using (2.1.7):

$$\frac{\partial(u^{(n)}d)}{\partial t}+\frac{\partial}{\partial n}(u^{(n)2}d+\tfrac{1}{2}d^2)+\frac{\partial(u^{(n)}u^{(s)}d)}{\partial s}=-d\frac{\partial h}{\partial n}+du^{(s)}+dF^{(n)} \qquad (3.5.3)$$

and

$$\frac{\partial(u^{(s)}d)}{\partial t}+\frac{\partial(u^{(n)}u^{(s)}d)}{\partial n}+\frac{\partial}{\partial s}(u^{(s)2}d+\tfrac{1}{2}d^2)=-d\frac{\partial h}{\partial x}-u^{(n)}d+dF^{(s)} \qquad (3.5.4)$$

These are the 'flux' forms alluded to above.

We can now proceed as before, integrating (3.5.3) and (3.5.4) across the shock and shrinking the integration interval to zero. Only the terms involving n- and t-derivatives remain finite, and thus (3.5.3) leads to

$$c^{(n)}\langle u^{(n)}d\rangle-\langle u^{(n)2}d+\tfrac{1}{2}d^2\rangle=0\,. \qquad (3.5.5)$$

[1] For a steady shock, it is easily shown that integration of (2.1.5) and (2.1.7) across the would yield conservation of the Bernoulli function, which would imply a lack of energy dissipation.

Note that (3.5.2) and (3.5.5) are identical to the conditions (1.6.4) and (1.6.5) governing one-dimensional shocks provided that the one-dimensional fluid velocity and shock speed are interpreted as $v^{(n)}$ and $c^{(n)}$. As a result, many of the properties of one-dimensional discontinuities apply locally to the two-dimensional, rotating discontinuities. For example, a stationary discontinuity requires that local normal velocity of the upstream state be 'supercritical' $u_u^{(n)} > (d_u)^{1/2}$ (*cf.* Equation 1.6.7).

The final matching condition is obtained by integration of (3.5.5), which yields

$$c^{(n)}\left\langle u^{(s)}d\right\rangle - \left\langle u^{(s)}u^{(n)}d\right\rangle = 0\,,$$

Together with (3.5.2), this result implies that the tangential velocity $u^{(s)}$ is conserved across the discontinuity:

$$\left\langle u^{(s)}\right\rangle = 0\,. \qquad (3.5.6)$$

The above matching conditions can also be found by simply considering the force and mass balances within a small box containing the shock, as shown in Figure 3.5.2a,b. The sides have length 2ε width $2l$ and the box extends from the bottom to the free surface. The box is fixed in space and is aligned so that its sides are parallel or perpendicular to *n*. The rate of change of *n*-momentum within the box must be balanced by the net flux of *n*-momentum into the box and the sum of the forces in the *n*-direction acting on the sides. One type of momentum flux is the normal flux $\left(u^{(n)}\right)^2$ across sides 1 and 2 of the box. Since $u^{(n)}$ is expected to be discontinuous across the shock, the difference in these normal fluxes remains finite as ε is decreased and but decrease in proportion to l as the l is decreased. Similarly, the depth-integrated pressure $\frac{1}{2}h^2$ over side 1 is different from that over side 2, even as ε as decreased. All other forces and fluxes go to zero more rapidly as the size of the box is decreased. For example, the tangential flux of normal momentum (the product $u^{(s)}u^{(n)}$) over sides 3 and 4 of the box are continuous in the *s*-direction and their difference decreases in proportion to εl as the box is shrunk. The Coriolis acceleration leads to a 'force' proportional to the integral of $du^{(s)}$ over the area of the box and is therefore proportional to εl. The same can be said for any contribution from bottom drag or topographic slope. Thus, as ε and l are decreased, the momentum budget reduces to

$$\frac{d}{dt}\iiint_V v\,dr \approx 2l\left[\tfrac{1}{2}(d_2^2 - d_1^2) + (d_2v_2^2 - d_1v_1^2)\right]$$

where V is the volume of the box. The left-hand integral reduces to $2lc^{(n)}(v_2^{(n)} - v_1^{(n)})$ as ε and l are reduced[2] and thus (3.5.5) is recovered.

The reader can appreciate that a similar treatment of the mass balance will lead to (3.5.2). The flux terms resulting from flow through sides 3 and 4 of the box are continuous and their difference therefore decreases more rapidly than the difference of the (discontinuous) normal flux terms ($v^{(n)}d$) as the box is shrunk. However the tangential momentum balance is more subtle, as suggested in Figure 3.5.2b. Here the leading contribution comes from the difference in the normal flux of tangential momentum, proportional to the difference in $u^{(s)}u^{(n)}$ between sides 1 and 2. The flux $\left(u^{(s)}\right)^2$ of tangential momentum and the pressure vary continuously between sides 3 and 4, and their difference leads to a negligible contribution as the box is shrunk. The same can be said for the contributions due to the Coriolis acceleration acting on the net normal velocity, the bottom drag, and topographic pressure. The result is that the change in net tangential momentum $c^{(n)}\left\langle u^{(s)}d\right\rangle$ is balanced by the difference in the normal flux of tangential momentum $\left\langle u^{(s)}u^{(n)}d\right\rangle$ as found above.

If $u^{(s)} \neq 0$ then the change in $u^{(n)}$ required by (3.5.1) implies that the velocity vector $\boldsymbol{u}=(u^{(n)},u^{(s)})$ must point in different directions on either side of a shock. Along a horizontal wall with free slip, the velocity vector is clearly aligned parallel to the wall regardless of whether a shock is present. These two facts can be reconciled only if C is aligned perpendicular to the wall at a point of contact, otherwise a flow into the boundary would be induced. In our slowly varying channel, where the walls are aligned in the y-direction, or nearly so, a shock must be aligned in the x-direction near the walls. One might now ask whether we can invoke the semigeostrophic approximation $v>>u$ right up to the shock, which would force the shock to lie in the x-direction all across the channel. If so, one could start with a specified, geostrophically balanced $v(y)$ and $d(y)$ immediately upstream of a hydraulic jump and use (3.5.1) and (3.5.4) to compute $v(y)$ and $d(y)$ immediately downstream. However, since the shock-joining conditions do not depend on the Coriolis parameter, there is no guarantee that the downstream v will be geostrophically balanced; in general it will not be so. In summary, the semigeostrophic equations are not generally valid right up the shock, nor must the shock remain aligned with x away from the channel walls. Since rotational effects generally require a finite distance (the deformation radius) over which to act, we anticipate the existence of a transitional region around the C within which the semigeostrophic flow away from C is adjusted to the (possibly) non-geostrophic flow at C.

This expectation is confirmed by the cross-stream momentum balance within the leading edge of the upstream-propagating 'Kelvin' bore of Figure 3.4.11. The momentum balance (Figure 3.5.3) is nearly geostrophic at t=20, but becomes less so with time. The primary source of contamination is the development of strong, cross-channel accelerations within the steepening regions of the bore, an effect evidenced by the growth of the term $\partial u / \partial t$. By t=80 the bore has steepened to the point where the depth changes

---

[2] A similar calculation was performed in connection with equation 1.6.8.

occur over a fraction of a deformation radius L_d $(=(gD_\infty)^{1/2}/f)$. However the ageostrophic region extends approximately 1/2 deformation radii upstream and downstream of the zone of rapid depth change.

Following the above remarks, one might expect a discontinuity in depth to occur within an ageostrophic region *R* that extends a distance O(L_d) downstream and possibly upstream (Figure 3.5.4). The 'shock' is now considered to be the whole region *R* with its imbedded discontinuity. *R* is joined upstream and downstream to semigeostrophic flows. It will be assumed that the flow in *R* is steady, but the same analysis can be carried out in the moving frame of shock that translates at a stead speed *c*. The central problem of shock joining is to predict the downstream semigeostrophic end state given the upstream end state (and, in the case of a moving shock, the speed *c*). If it is the case that the potential vorticity distribution $q(\psi)$ is preserved as the flow passes through *R*, then the shock joint problem is straightforward. For the $q(\psi)$ given by the known upstream condition, the downstream end state is found by solving the second order equation (2.2.2). The resulting profile of downstream depth, and the corresponding geostrophic velocity would then be know within two integration constants. These constants could be determined by two additional constraints, one being conservation of the total volume flux. A second constraint is provided by the conservation of the total (width integrated) flow force:[3] : $\int_{-w/2}^{w/2}\left[v^2 d+\frac{1}{2}d^2\right]dx$. In summary, the conservation of volume flux, $q(\psi)$, and total flow force through *R* should be sufficient to close the shock joining problem.

Success of this procedure depends on potential vorticity conservation across the discontinuity, and we now ask whether this is consistent with (3.5.2, 3.5.5 and 3.5.6). Using the fact that Bernoulli function and potential vorticity are related by $q=dB/d\psi$, where ψ represents the streamfunction of the steady flow seen in the frame of reference moving with the steadily propagating shock. Since mass is conserved across the discontinuity, we have $\langle d\psi\rangle = 0$ and therefore

$$\langle q\rangle = \left\langle \frac{dB}{d\psi}\right\rangle = \frac{\langle dB\rangle}{d\psi}. \tag{3.5.7}$$

In addition, the jump in the value of *B* can be written in terms of the jump in depth using the previously derived relation (1.6.6) for energy dissipation, nondimensionally expressed as

$$\langle B\rangle = -\frac{\langle d\rangle^3}{4d_d d_u}. \tag{3.5.8}$$

[3] The width-integrated flow force is concerved provided the horizontal component of bottom or side-wall pressure within *R* is not important. In a gradually varying channel, the length scale *L* of topographic and width variations is large compared to the length L_d of *R* and therefore the bottom and side-wall pressure alter the momentum flux through *R* by only an O(L_d/L) amount.]

Here d_d and d_u are the depths immediately upstream and downstream of the discontinuity at the point of interest. Thus

$$\langle q \rangle = -\frac{d}{d\psi}\frac{\langle d \rangle^3}{4d_d d_u} = \frac{1}{[u^{(n)}d]_{u \text{ or } d}}\frac{d}{ds}\frac{\langle d \rangle^3}{4d_d d_u} \qquad (3.5.9)$$

where s represents distance measured along the shock as shown in Figure 3.5.4. The normal velocity $u^{(n)}$ is that seen in the moving frame. An observer facing the shock from upstream sees a positive normal velocity entering the shock, with ψ decreasing, and s increasing, from right to left. The dimensional version of (3.5.9) is obtained by multiplying its right-hand side by g and regarding all other variables as dimensional.

Nof (1986) presents a special class of shocks that can be described analytically and for which the potential vorticity change can be calculated. The procedure is to look for a solution in which the channel flow is parallel (v=0), and therefore geostrophic, right up to the discontinuity. The latter is assumed to be aligned in the x-direction so that C consists of a straight line perpendicular to the channel axis (Figure 3.5.5). Under the restrictions that both end states are parallel, and therefore geostrophically balanced, and that (3.5.2, 3.5.5, and 3.5.6) are satisfied at each x, a special class of upstream states can be found that permit stationary shocks with the assumed properties. As noted above, the upstream state must be 'locally supercritical' $v>d^{1/2}$ at each y. The results are classified in terms of two parameters: a Froude number $F_w = v_u\big|_{x=w/2} / d_u^{1/2}\big|_{x=w/2}$ and Rossby number $v_u(w/2)/w$, both based on right-wall values of the upstream flow. Figure 3.5.6 has some sample solutions showing the upstream and downstream depths. Starting with the value F_w=0, where there is no discontinuity, the jump $\langle d \rangle$ in depth across the shock tends to increase as F_w increases. For individual solutions, $\langle d \rangle$ tends to increase from left-to-right and, according to (3.5.9), this is consistent with an increase in potential vorticity for the fluid passing through the discontinuity. The computed increases are shown in Figure 3.5.7 for a particular value of $v_u(w/2)/w$. Note that these changes can be O(1). Potential vorticity changes are present in the Kelvin wave jump of Figure 3.30.

The non-conservation of potential vorticity across a shock can give rise to interesting downstream effects including jets and vortex streets. Consider a nonrotating jump in a channel with a rounded cross-section (Figure 3.5.8). This feature was studied modeled by Siddall et al. (2004) as part of a simulation of an ancient flood thought to occur into the Black Sea. The upstream flow is parallel and uniform (v=0, u=constant) and therefore q_u=0. The jump involves an increase in the (level) free surface and ($d_d(s) - d_s(s)$) is therefore constant. The differentiated term on the right-hand side of (5.3.9) is therefore controlled by the denominator, which decreases to the left and right of the channel center. The differentiated term therefore increases away from the channel center and it follows that q_d>0 to the left and q_d<0 to the right. With the neglect of f, q_d is proportional to the vorticity of the fluid downstream of the jump, the distribution of which is consistent with a jet-like velocity profile, as produced by a numerical simulation (Figure 3.5.9).

Equally important and closely related to potential vorticity change is the production of vorticity within a shock. A helpful form of the vorticity equation (see Exercise 1 or Section 2.1) is

$$\frac{\partial \zeta_a}{\partial t} + \nabla \cdot \left[\mathbf{u}\zeta_a + \mathbf{J}_n \right] = 0 , \qquad (3.5.10)$$

which is derived by taking the curl of the momentum equations (2.1.1 and 2.1.2) and using (2.1.3). In this dimensionless form, $\zeta_a = 1 + \zeta$ is the absolute vorticity and $\mathbf{J}_n = \mathbf{k} \times \mathbf{F}$, where $\mathbf{F}$ contains the dissipation and horizontal body force. For the flows under consideration, the later is generally zero and we will think of $\mathbf{J}_n$ as arising only from dissipation. The vorticity flux vector $\mathbf{u} \cdot \zeta_a + \mathbf{J}_n$ is then composed of an advective part $\mathbf{u} \cdot \zeta_a$ plus a dissipative part.

Taking the cross-product of **k** with the steady version of (2.1.15) yields

$$\mathbf{k} \times \nabla B = \mathbf{u}\zeta_a + \mathbf{J}_n , \qquad (3.5.11)$$

which shows that the Bernoulli function acts as a streamfunction for the vorticity flux (Schär and Smith, 1993)[4]. Since **u** is parallel to streamlines, the derivative of B along streamlines gives a contribution that is entirely due to dissipation. If the dissipation is zero, the vorticity flux is entirely due to advection and is proportional to the derivative of B in the cross-streamline direction. In the treatment of shocks we generally consider the dissipation to be negligible outside the region of rapid or discontinuous change.

A nice application of these ideas is to atmospheric wakes in the lee of islands and mountains (e.g., Smith et al. 1997). For the islands in question, the effects of the Earth's rotation are generally weak. The reduced airflow in the wake reduces the sea surface roughness, resulting in 'shadows' in the sunglint patterns (e.g. Figure 3.5.10). In an idealized view of the wake, the winds approaching the island are uniform and are confined to a shallow surface layer that obeys the reduced-gravity version of our shallow water equations. When the approach flow is subcritical and the island is not so high that it protrudes through the upper interface, the fluid spilling over the top can become supercritical and form a hydraulic jump (Figure 3.5.11). Regions of cyclonic and anticyclonic shear are also observed downstream of the jump and these are indicated in the figure. In some cases the vorticity is collected in a vortex street, a train of staggered eddies of alternating sign (Figure 3.5.12). If the approach flow is uniform and inviscid, the downstream vorticity must be generated by the jump.

[4] The inviscid form of (3.5.11) is related to a more general result obtained by Crocco (1937).

The discontinuity in depth is largest at the center (y=0) of the jump and (3.5.8) suggests that the loss in Bernoulli function should also be largest there. The flow immediately downstream of the jump should therefore have a minimum in B at x=0 and B should increase as one moves along the jump in either direction (to the right of left, facing downstream). It is also assumed that B is conserved along streamlines ($\mathbf{J}_n$=0) in the downstream region, changes having already taken place where the streamline passed through the jump. The y-component of (3.5.11) for the flow $\partial B / \partial x = v\zeta_a$ immediately downstream of the jump is $\partial B / \partial x = v\zeta_a$, where v>0 and $\partial B / \partial x$ is >0 for x>0 and is <0 for x<0. The vorticity ζ_a, which is dominated by the relative vorticity ζ in these applications is therefore positive on the right-hand side of the wake (facing downstream) and negative on the left side. Since the approach flow has zero vorticity, the positive and negative vorticity must have been generated within the jump and could account for the vorticity in the alternating eddies.

A complementary result can be found by applying (3.5.11) to the interior of the jump itself. To do so, it must be assumed that the rapid change in depth occurs over a small but finite distance and that (3.5.11) continues to hold within. Consider the component of this equation tangential to the jump. If one temporarily consider x to be the tangential direction, then this component is given by $-\partial y / \partial y = u\zeta_a + J^{(x)}$. Integration of this relation across the small interval ($-\varepsilon \leq y \leq \varepsilon$, say) of rapid depth change yields

$$\int_{-\varepsilon}^{\varepsilon} (u\zeta + J_n^{(x)})dy = -(B|_{x=\varepsilon} - B|_{x=-\varepsilon}) > 0 \,.$$

The left hand term can be interpreted as a vorticity flux tangent to the jump, positive in the left to right direction (facing downstream). Its magnitude is zero at the extremities of the jump and therefore its divergence is positive over the left portion and negative over the right portion. A positive divergence is consistent the generation of negative vorticity in the jump, whereas a convergent flux indicates a generation of positive vorticity. Both tendencies are in agreement with the vorticity carried away from the jump by the fluid.

Exercises

1. Deduce the inviscid form of (3.5.11) directly from the relation $q=dB/d\psi$?

2. For the nonrotating hydraulic jump shown in Figure 3.5.11 in which the depth is maximum at the centerline and the upstream velocity is uniform across the channel, show that the change in potential vorticity produces a downstream vorticity distribution (cyclonic on the left and anticyclonic on the right side of the channel) consistent with a jet.

Figure Captions

Figure 3.5.1 Definition sketch showing discontinuity in depth ***C*** that moves normal to itself at speed $c^{(n)}$ at the point *P*.

Figure 3.5.2 Control volumes (viewed from above) with (a) fluxes of momentum normal to the jump and (b) fluxes of momentum tangential to the jump.

Figure 3.5.3 The frames on the left show the longitudinal sections of the surface elevation for the flow of Figure 3.30 at various times. The three sections in each frame are taken at the channel centerline and walls: x=0 and $x=\pm w/2$. The frames on the right show the terms in the y-momentum balance at the channel centerline over the interval indicated by vertical bars in the corresponding figure to the right.

Figure 3.5.4 Idealized view of the ageostrophic region *R* and the imbedded depth discontinuity.

Figure 3.5.5 The shock hypothesized by Nof (1986). The depth discontinuity is perpendicular to the channel walls and the parallel, geostrophically balanced, upstream and downstream flows join directly to the discontinuity. (There is no adjustment region.)

Figure 3.5.6 Upstream and downstream depth profiles for a shock of the type shown in Figure 3.5.5. The governing upstream parameters are a Froude number $F_w = v_u(w/2)/d_u^{1/2}(w/2)$ and Rossby number $v_u(w/2)/w$, both based on values at the right channel wall ($x=w/2$). The value of the latter for all plots shown is 0.2. (Nof 1986, Figure 7.)

Figure 3.5.7 The change in potential vorticity across the shocks shown in Figure 3.5.6. (Nof, 1986, Figure 10.)

Figure 3.5.8 Schematic of a nonrotating hydraulic jump produced in a channel with a parabolic bottom. (Figure 7 of Siddall, et al. 2004).

Figure 3.5.9 Plan view of the jump suggested in Figure 3.5.8, as produced in a numerical simulation. The sudden change in depth occurs within the dashed area. The arrows indicate the depth-integrated velocity. (Figure 8 of Siddall, 2004).

Figure 3.5.10 Satellite photo showing sea surface glint around the Windward Islands. (NASA image S1998199160118, free of licensing fees but NASA ownership must be acknowledged)

Figure 3.5.11 Idealized plan view of hydraulic jump and wake in the lee of an obstacle (Schär and Smith, 1993, Figure 2).

Figure 3.5.12 Landsat 7 image of a vortex street as apparent in the cloud cover off the Chilean coast near the Juan Fernandez Islands on September 15, 1999. (NASA image Vortex-street-1.jpg.)

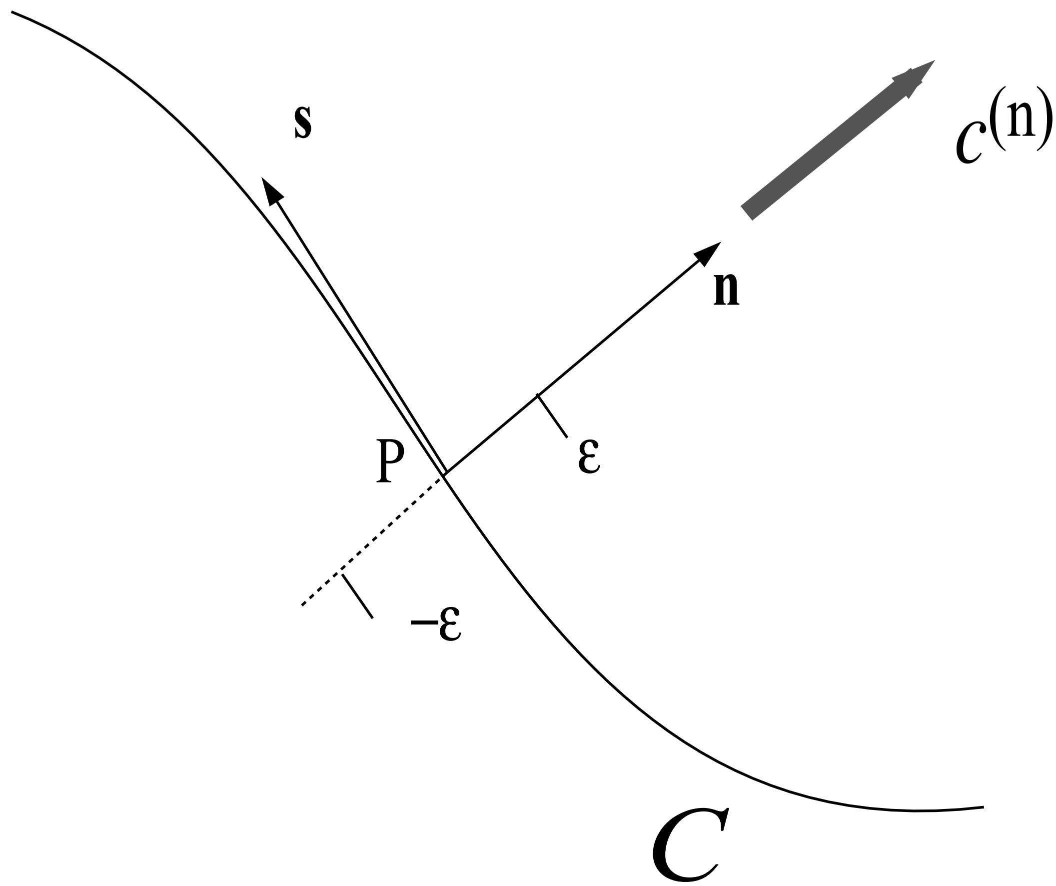

Figure 3.5.1

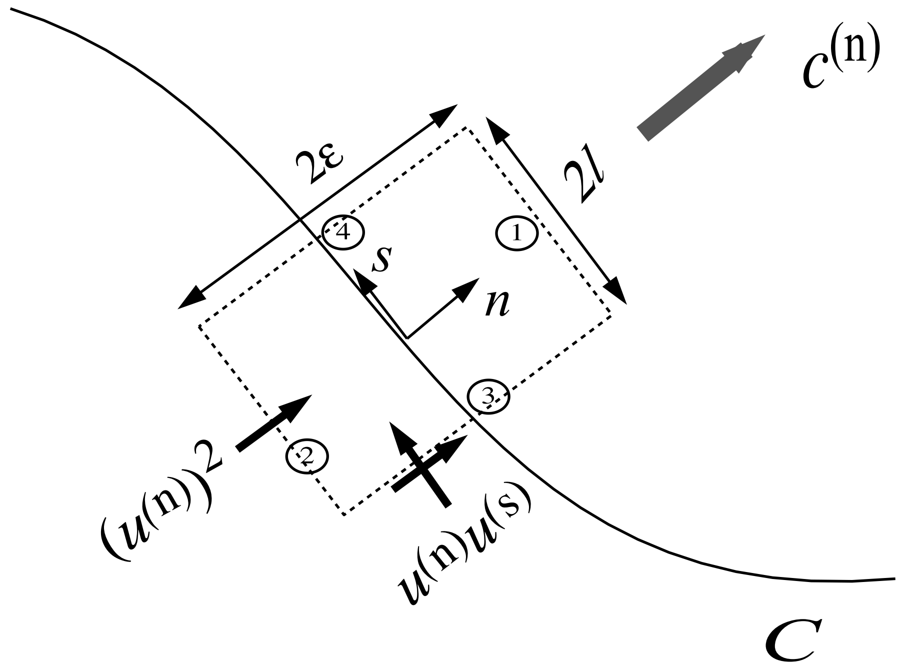

(a)

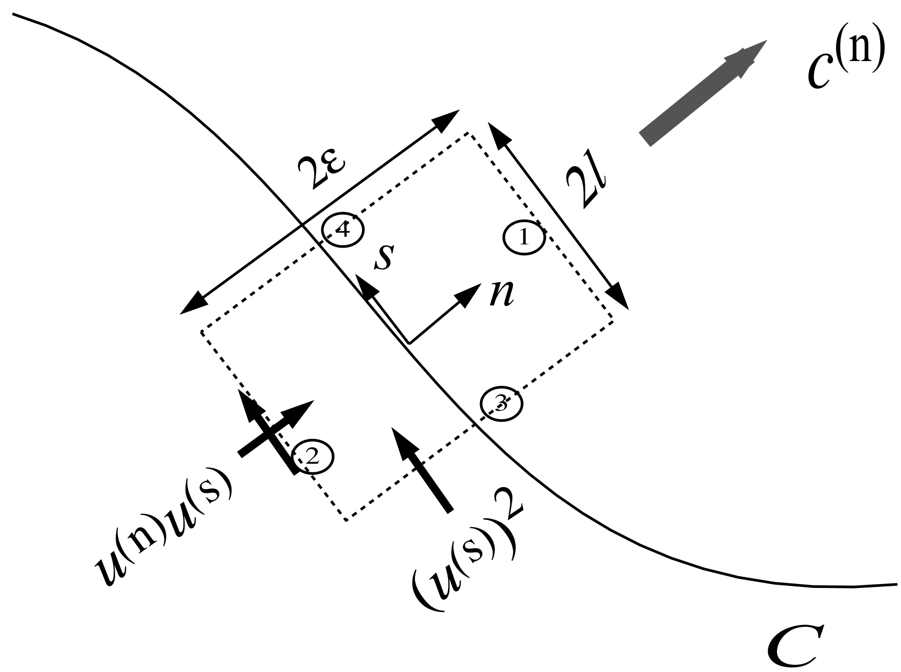

(b)

Figure 3.5.2

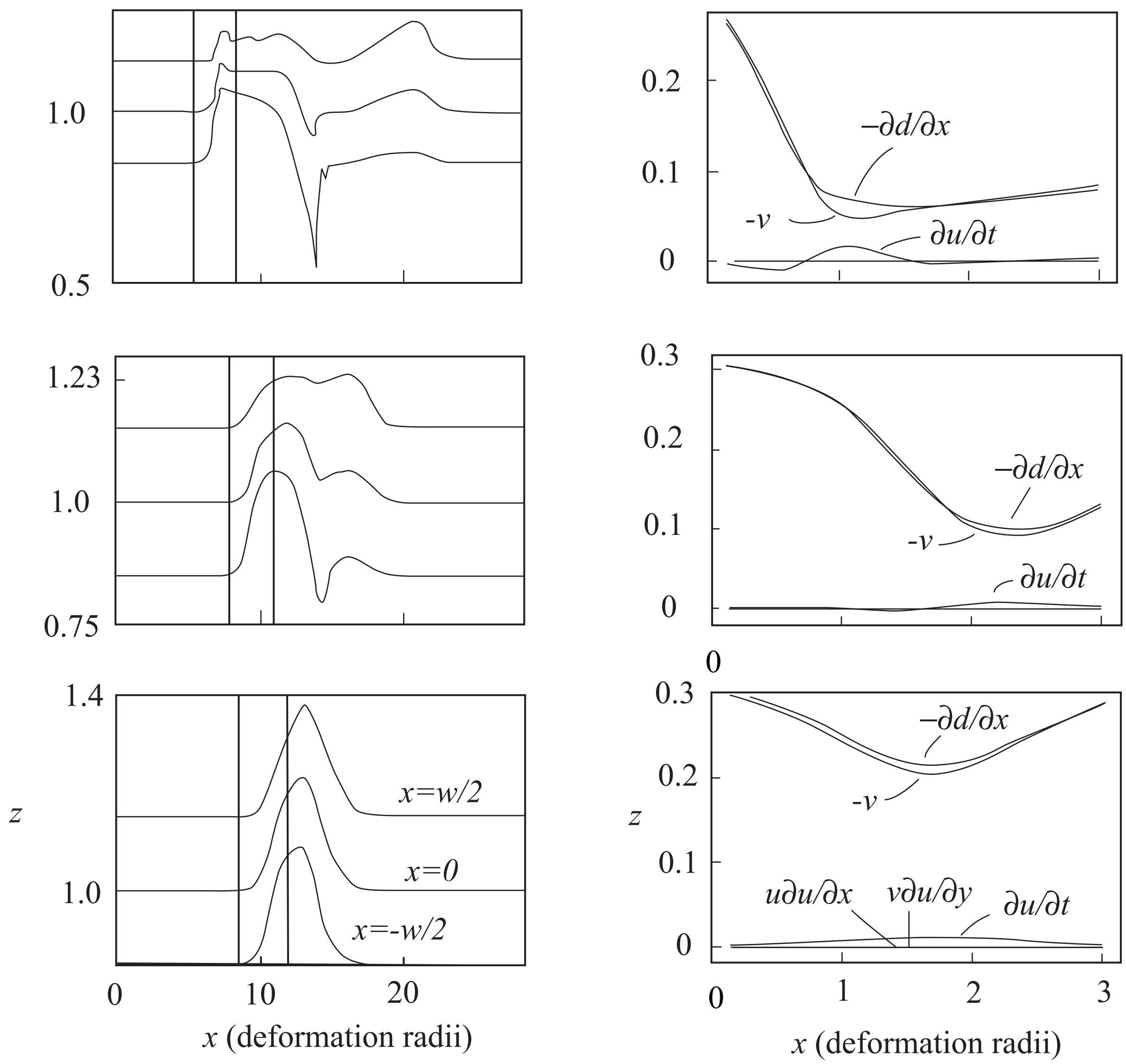

Figure 3.5.3.cs2.ai

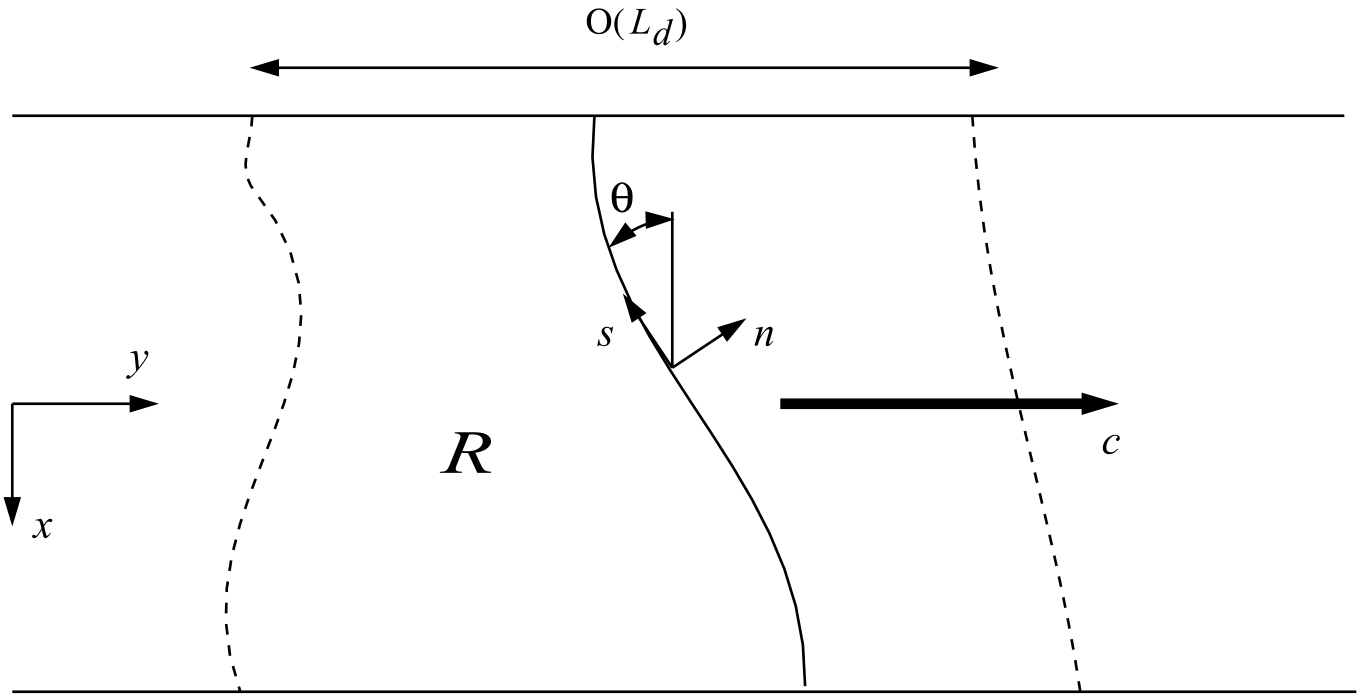

Figure 3.5.4

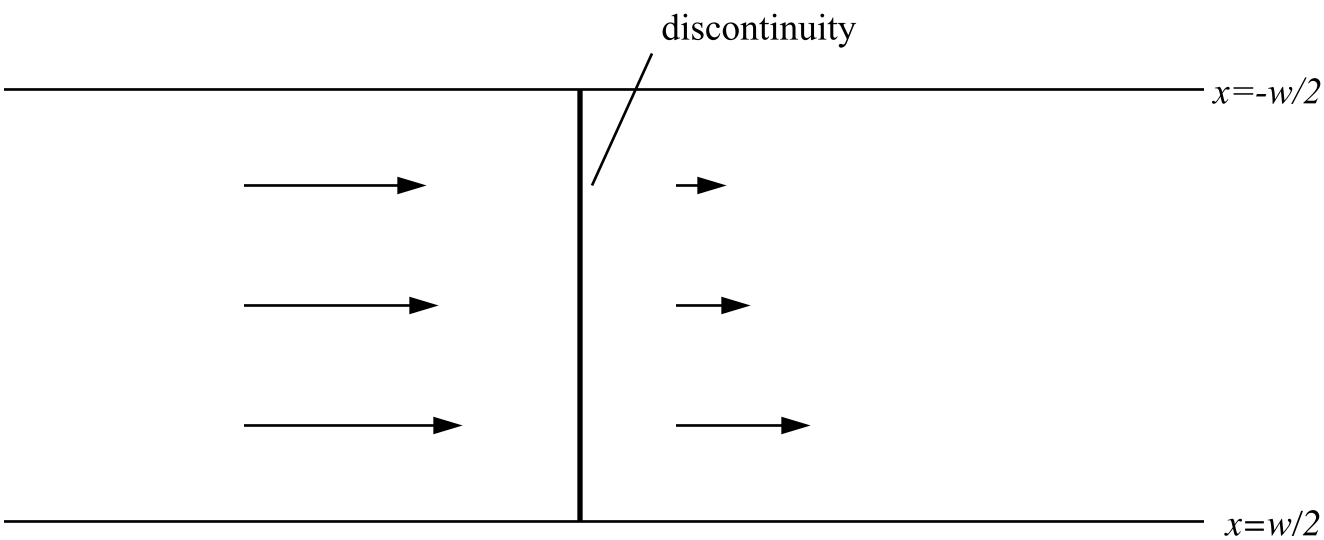

Figure 3.5.5

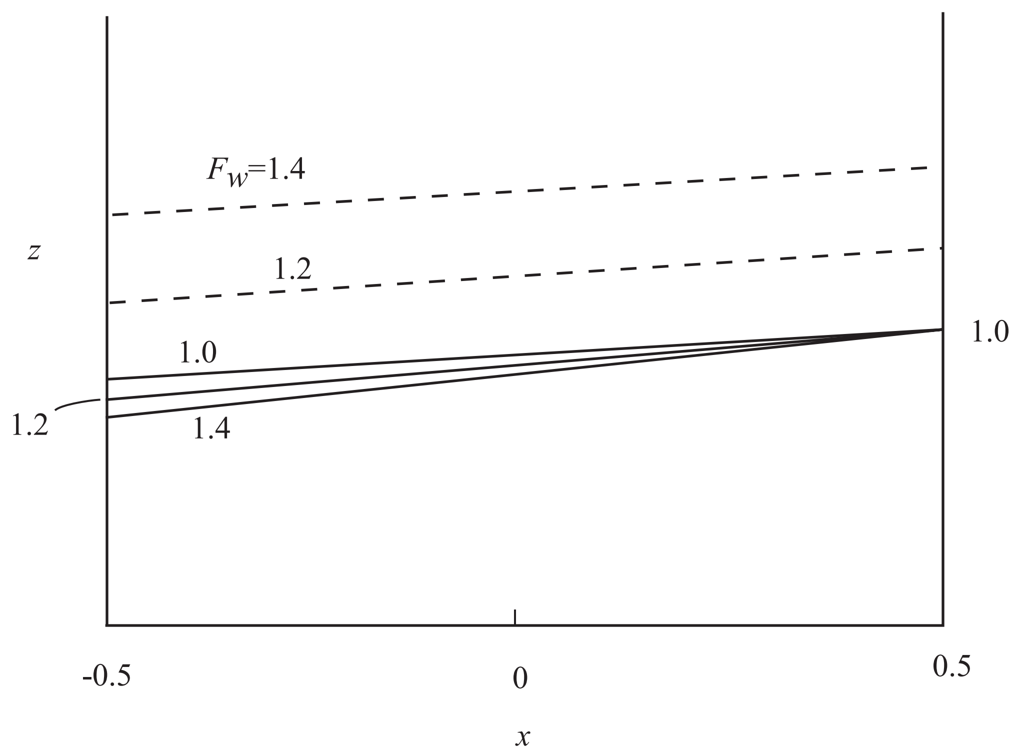

Figure 3.5.6

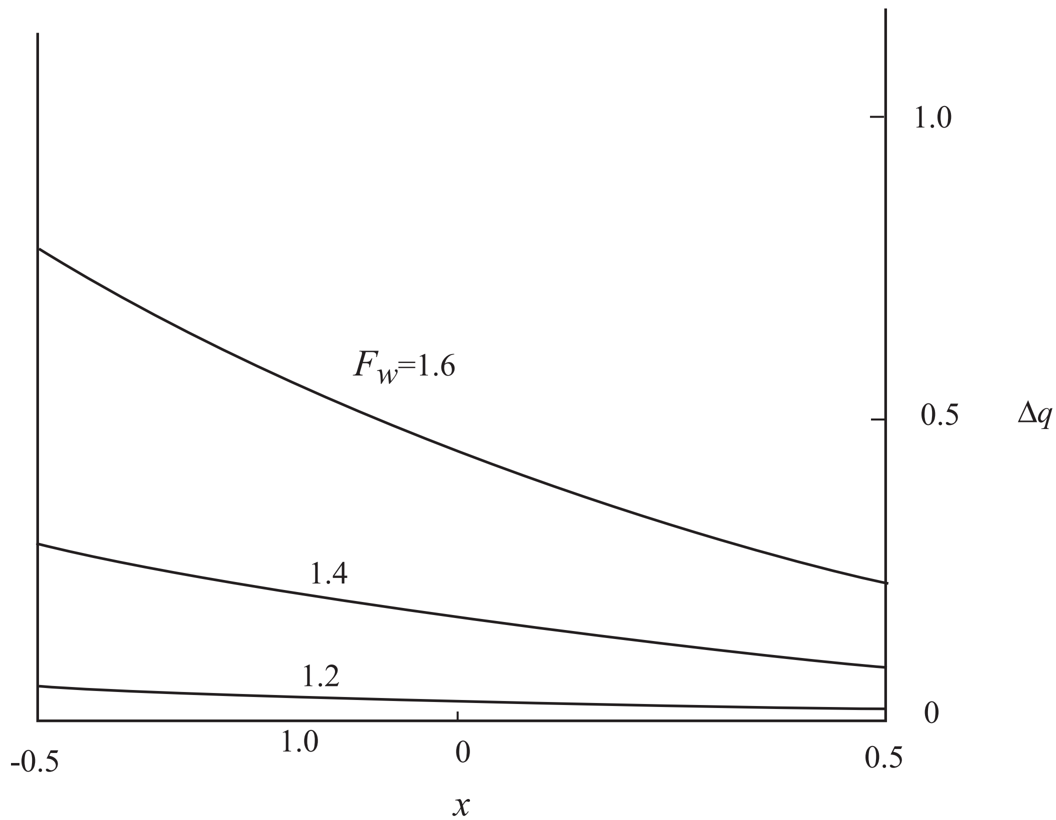

Figure 3.5.7

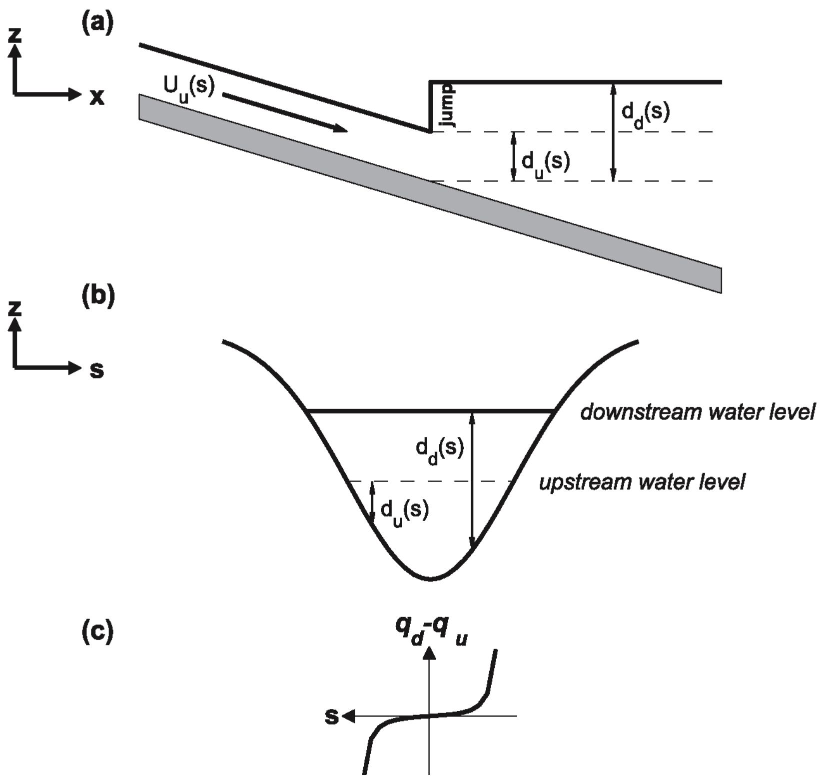
(a)
z
x
$U_u(s)$
jump
$d_d(s)$
$d_u(s)$
(b)
z
s
downstream water level
$d_d(s)$
upstream water level
$d_u(s)$
(c)
q_d-q_u
s

Figure 3.5.8

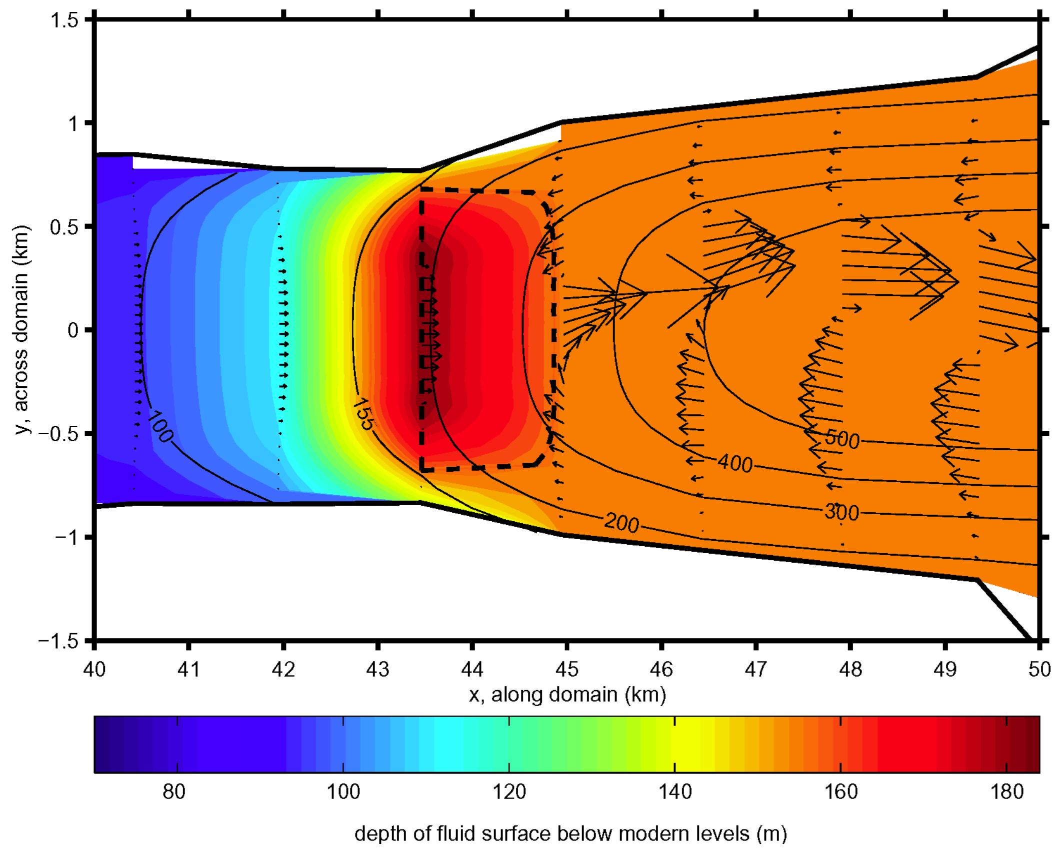

1.5
1
0.5
0
−0.5
−1
−1.5
y, across domain (km)
40
41
42
43
44
45
46
47
48
49
50
x, along domain (km)
100
155
200
300
400
500
80
100
120
140
160
180
depth of fluid surface below modern levels (m)

Figure 3.5.9

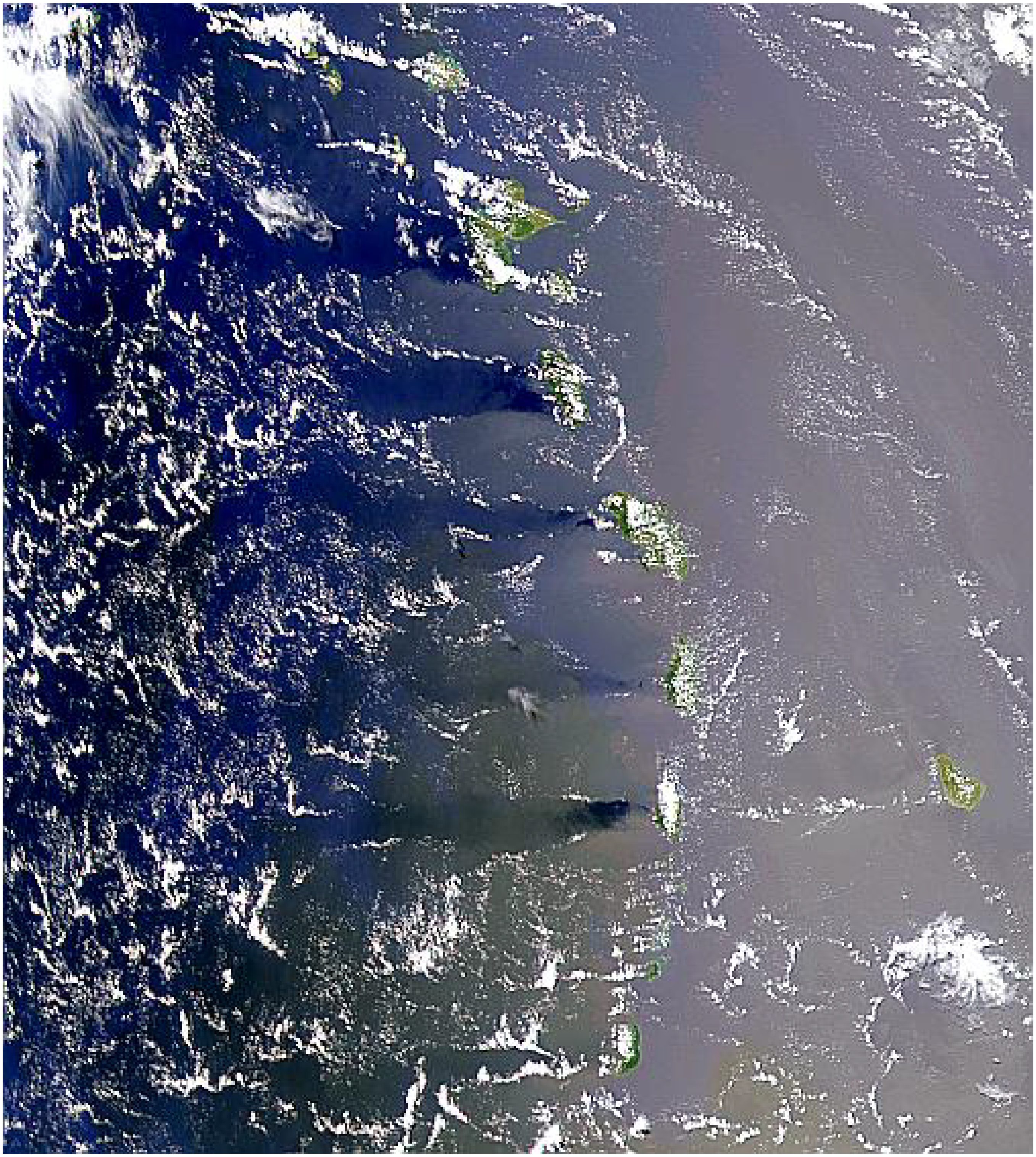

Figure 3.5.10

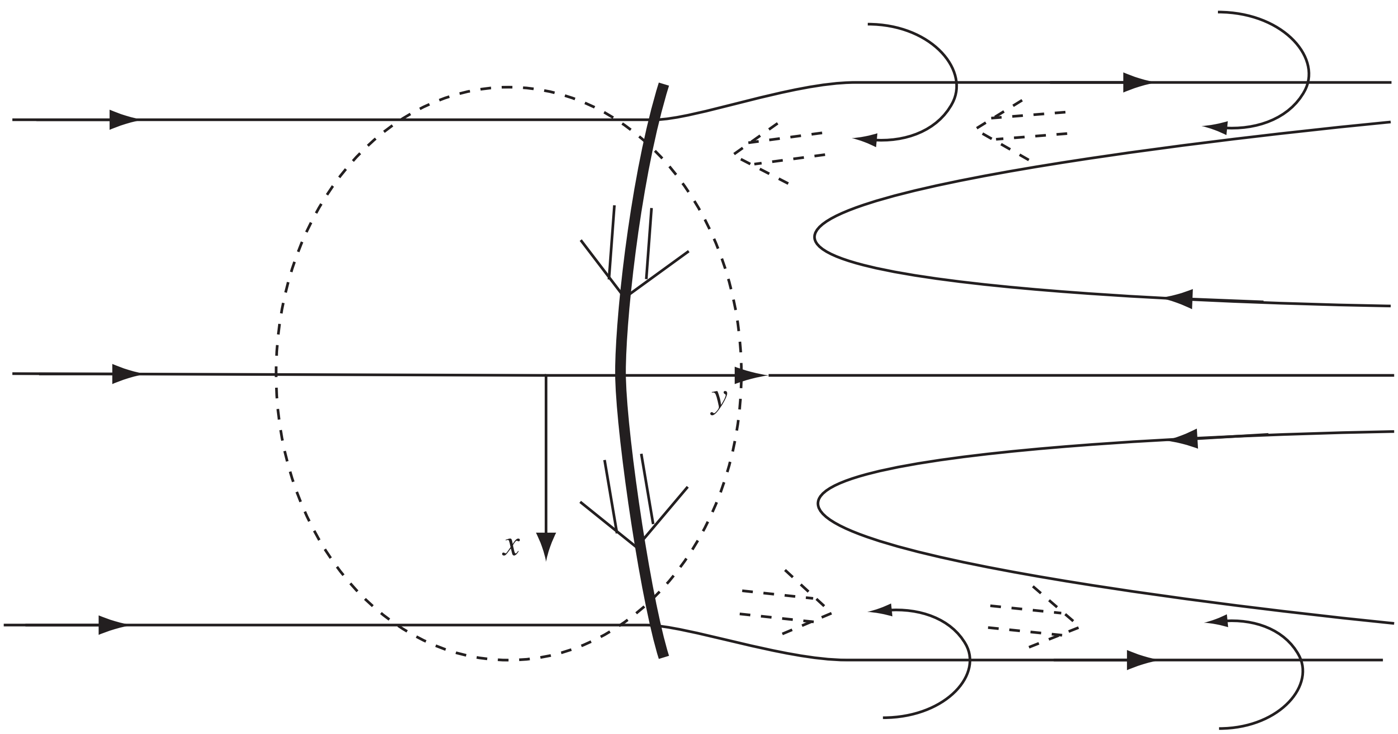

Figure 3.5.11

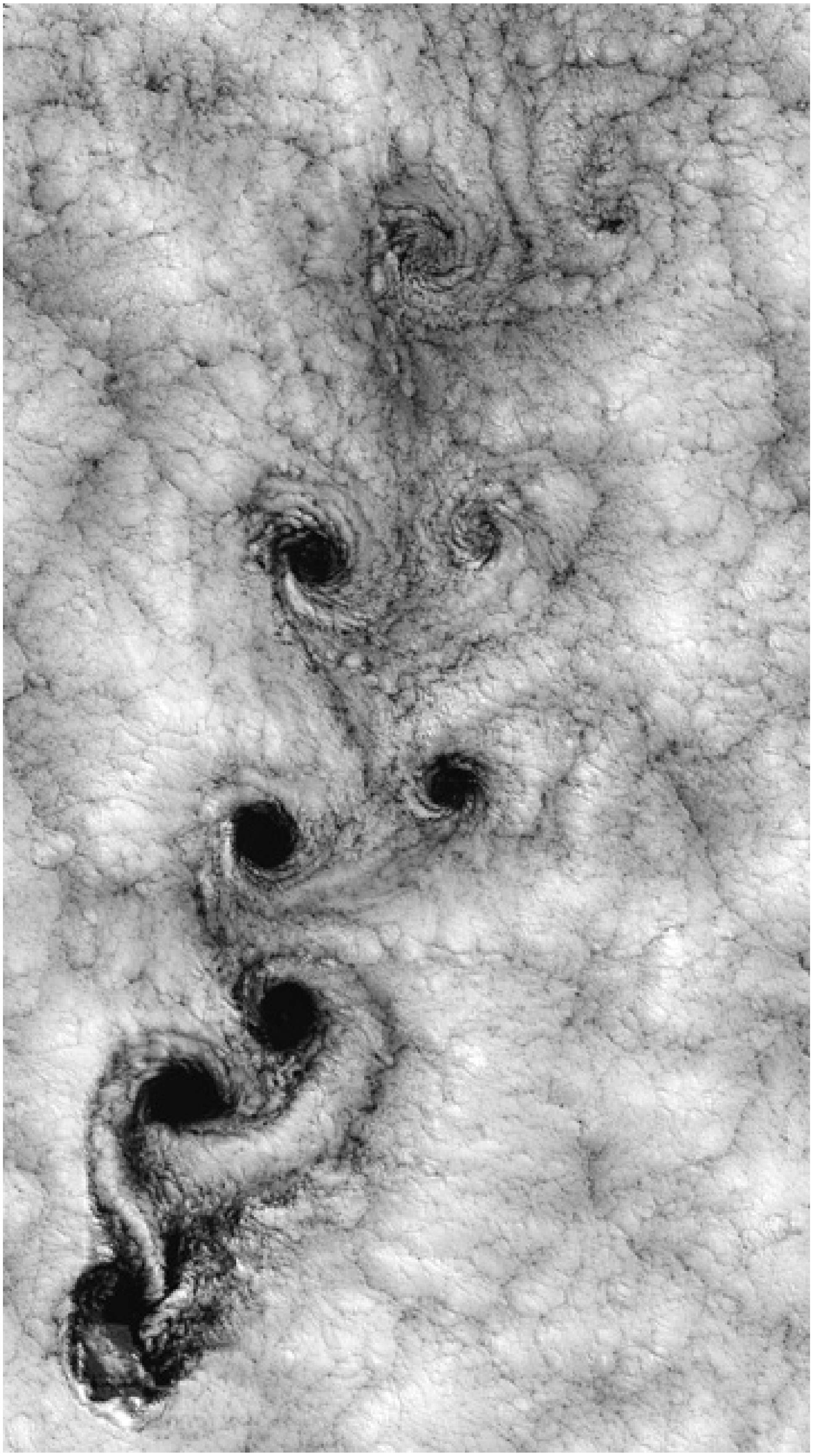

Figure 3.5.12 (low resolution version)